ORIGINAL ARTICLE

Involvement of microRNA-23b in TNF-α-reduced BMSC osteogenic differentiation via targeting runx2

Lin Deng[1] · Guoli Hu[2] · Lei Jin[3] · Chenglong Wang[4] · Hongwen Niu[1]

Abstract

Elucidation of the molecular mechanism governing bone marrow mesenchymal stem cell (BMSC) osteogenic differentiation is of great importance for improving the treatment of osteoporosis. TNF-α is a well-known inhibitory factor during osteogenic differentiation of BMSCs. In our experiment, we consistently observed that TNF-α significantly inhibited BMSC osteogenic differentiation, which was partially rescued by BAY 11-7082 (NF-κB inhibitor). In this study, we examined the potential roles of microRNAs (miRNAs) involved in TNF-α-mediated reduction of BMSC osteogenesis. We found that microRNA-23b (miR-23b) was dramatically induced under the stimulation of TNF-α, which was abolished by BAY 11-7082. Similar to the effect of TNF-α, miR-23b agonist (agomir-23b) obviously impaired BMSC osteogenic differentiation in vitro and in vivo. However, agomir-23b had no effect on osteoclast activity. Overexpression of miR-23b significantly reduced runx2, the master transcription factor during osteogenesis, suggesting that miR-23b acts as an endogenous attenuator of runx2 in BMSCs. Mutation of the putative miR-23b binding site in *runx2* mRNA blocked miR-23b-mediated repression of the *runx2* 3′ untranslated region (3′UTR) luciferase reporter activity, suggesting that miR-23b directly binds to *runx2* 3′UTR. Furthermore, infection with Ad-*runx2* (adenovirus carrying the entire CDS sequence of runx2) effectively rescued the inhibition of BMSC osteogenic differentiation in miR-23b-overexpressing cells, indicating that the inhibiting effect of miR-23b on osteogenesis is mediated by suppression of runx2. Moreover, caudal vein injection of agomir-23b notably caused severe osteoporosis in mice, and forced expression of runx2 by combined injecting Ad-*runx2* attenuated the bone loss induced by miR-23b. Collectively, these data indicated that miR-23b was involved in TNF-α-mediated reduction of BMSC osteogenesis by targeting runx2. These findings may provide new insights into understanding the regulatory role of miR-23b in the process of BMSC osteogenic differentiation in inflammatory conditions and a novel therapeutic target for osteoporosis.

Keywords MiR-23b · Runx2 · TNF-α · BMSCs · Osteogenic differentiation

Lin Deng and Guo-Li Hu contributed equally to this work.

✉ Hongwen Niu
shuguang3138@163.com

1 Department of Traumatology, Shu Guang Hospital Affiliated to Shanghai University of Traditional Chinese Medicine, Shanghai, China

2 Key Laboratory of Stem Cell Biology, Institute of Health Sciences, Shanghai Jiao Tong University School of Medicine (SJTUSM) and Shanghai Institutes for Biological Sciences (SIBS), Chinese Academy of Sciences, Shanghai, China

3 Anorectal Surgery, Shanghai Min Hang Traditional Chinese Medicine Hospital, Shanghai, China

4 Department of Orthopedic Surgery, Xin Hua Hospital Affiliated to Shanghai Jiao Tong University School of Medicine (SJTUSM), Shanghai, China

Introduction

Bone mass regulation depends on the dynamic balance between bone formation and bone resorption, which are driven by osteoblast activation and osteoclast activation, respectively [1]. As a major constituent of bone, osteoblasts are essential for maintaining skeletal architecture and modulating bone microenvironment homeostasis. Osteoblasts have been well-documented to produce a variety of extracellular matrix proteins, including osteocalcin (OCN), alkaline phosphatase (ALP), osteopontin (OPN) and type I collagen [2].

Osteogenesis is an active process initiated by mesenchymal stem cells (MSCs) [3], which are stromal cells with multi-potency and can fully differentiate towards various cell types such as osteoblasts, chondrocytes and adipocytes [4, 5]. This process occurs throughout life and is involved

in bone remodeling in adults [6], and it is also regulated by inflammatory cytokines, such as TNF-α, which has been shown to inhibit osteoblast differentiation and bone formation in multiple models [7, 8]. TNF-α has been considered as one of the major cytokines responsible for bone loss in many bone-related inflammatory diseases [9, 10]. In addition, TNF-α negatively regulates Wnt signaling in bone marrow mesenchymal stem cells (BMSCs), which mediate the inhibitory effect of TNF-α on osteogenic differentiation [11, 12].

MicroRNAs (miRNAs) are endogenous, small (19–25 nt), non-coding RNAs that regulate their targets by incomplete complementation to nucleotides within the 3′ untranslated region (3′UTR) or open reading frame (ORF) of coding mRNAs, resulting in suppressing gene expression by inhibiting translation, promoting mRNA decay or both [13]. MiRNAs have emerged as key regulators of various biological and pathological processes [14]. Previous studies have shown that miR-204, miR-135b and miR-208 present with similar inhibitory effect on BMSC osteogenic differentiation [15–17]. On the contrary, miR-194 and miR-216a have been demonstrated to promote BMSC osteogenesis [18, 19]. Meanwhile, the impact of miRNAs on osteogenic differentiation of other cell types has also been examined by modulation of miRNA function [20], indicating the significant importance of miRNA regulation on this biological process.

Recently, microRNA-23b (miR-23b) has been reported to regulate the balance between osteoblast and adipocyte differentiation in BMSCs [21]. In addition, downregulated miR-23b promotes BMP9-mediated osteogenesis in C2C12 myoblast cells [22]. However, the regulatory role of miR-23b in the process of osteogenic differentiation of BMSCs in an inflammatory condition remains ambiguous. In the present study, we showed that miR-23b was sensitive to TNF-α, characterized by a prompt increase upon the stimulation of TNF-α. TNF-α induced the expression of miR-23b mainly through a canonical NF-κB signaling pathway. In turn, TNF-α-induced miR-23b significantly decreased runx2 in BMSCs, resulting in the inhibition of BMSC osteogenic differentiation in vitro and in vivo. Interestingly, overexpression of runx2 by Ad-*runx2* efficiently rescued miR-23b-reduced BMSC osteogenic differentiation. On the other hand, agomir-23b had no effect on osteoclast activity. Furthermore, in vivo, agomir-23b obviously caused severe osteoporosis by caudal vein injection. In summary, miR-23b was involved in TNF-α-inhibited BMSC osteogenic differentiation mechanically through suppressing runx2, and miR-23b-induced bone loss was mainly attributed to lack of BMSC-derived osteoblasts but not bone resorption. Our findings illuminate the regulatory role of miR-23b in the process of osteogenic differentiation in an inflammatory condition and provide a novel potential therapeutic target for osteoporosis.

Materials and methods

Cell culture and transfection

Bone marrow from the femurs of each donor was aspirated and collected in a 10-cm dish containing modified Eagle's medium (MEM; #51412C; Sigma-Aldrich) with 10% fetal bovine serum (#A15–204; PAA, Pasching, Austria), 100 U/mL penicillin G, and 100 mg/L streptomycin (#15070–063; Life Technologies, Carlsbad, CA, USA). The cells were cultured at 37 °C with 5% CO_2. After cell culturing for 48 h, non-adherent cells were removed by washing with phosphate-buffered saline (PBS). The adherent cells were cultured in a complete medium that was replaced every 2 days. After achieving 80% confluence, the cultures were digested with 0.25% trypsin/ethylene diaminetetraacetic acid (EDTA; #25200-056; Life Technologies). The cells at passages 2–6 were used for the following experiments. For TNF-α stimulation experiments, hBMSCs were treated with TNF-α (10 ng/mL) for 24 h. For transfection of miRNA, the medium was transfected by Lipofectamine2000 (Invitrogen, MA, USA) according to the manufacturer's instructions. Agomi-23b (Guangzhou Ribo Bio Co., Ltd.) was transfected at a concentration of 200 nM. The agomir and negative control sequences: Ago-23b, 5′-AUCACAUUGCCAGGGAUU ACC-3′; NC, 5′-UUGUACUACACAAAAGUACUG-3′.

Identification of hBMSCs

Human BMSCs (hBMSCs, 5×10^5 cells) at passage 3 were incubated with 1 μg of phycoerythrin conjugated or fluorescein isothiocyanate-conjugated mouse anti-human monoclonal antibodies (R&D Systems, Minneapolis, MN, USA) for 45 min at room temperature. After washing with fluorescence-activated cell-sorting (FACS) buffer (PBS with 10% bovine serum albumin and 1% sodium azide) at 376 g for 5 min, the stained cells were resuspended in 300 mL of ice-cold FACS buffer and subjected to flow cytometry analysis (BD Biosciences, San Jose, CA, USA). A total of 104 events were counted for each sample. The percentage of cells with a positive signal was calculated using the technical flow cytometry. The antibodies used in the present study included CD-44 (#555478; BD Pharmingen), CD-90 (#551401; BD Pharmingen), CD-34 (#555822; BD Pharmingen) and CD45 (#340953; Biosciences).

Induction of hBMSCs

For osteogenic differentiation assays, hBMSCs seeded at 1×10^4 cells/cm^2 were cultured in a complete culture medium until confluent. Then, the hBMSCs were incubated

in basal medium (α-MEM with 10% fetal bovine serum, 100 U/mL penicillin G, and 100 mg/L streptomycin) or osteogenic medium [basal medium supplemented with 1 nM dexamethasone (#D4902; Sigma-Aldrich), 50 mM ascorbic acid (#A4403; Sigma-Aldrich), and 20 mM beta-glycerolphosphate (#G9891; Sigma-Aldrich)] for 14 days for the assessment of alizarin red S (#A5533; Sigma-Aldrich) staining. For alizarin red S staining, the cultured cells were rinsed with PBS three times and fixed with 4% paraformaldehyde for 10 min at room temperature. The fixed cells were then soaked in 0.5% alizarin red S for 30 min at room temperature, washed with PBS, and then observed under a digital camera (IXUS 115 HS; Canon, Tokyo, Japan).

For chondrogenic differentiation assays, hBMSCs were harvested and resuspended at a density of 1×10^7 cells/mL. A total of 20 µL of cell suspension was carefully placed in the interior of a 12-well plate. The cells were allowed to adhere at 37 °C in 5% CO_2 for 2 h, followed by the addition of 500 µL of chondrogenic medium that contained basal medium, which was supplemented with 10 ng/mL of recombinant human transforming growth factor beta 1 (#7666-MB-005; R&D Systems) and 50 ng/mL recombinant human insulin-like growth factor 1 (#6630-GR-025; R&D Systems). The cells were fixed for alcian blue staining (#A3157; Sigma-Aldrich) after 21 days.

For adipogenic differentiation assays, hBMSCs (1×10^4 cells/cm^2) were cultured in a complete culture medium. After 2 days, the medium was replaced with basal or adipogenic medium, wherein the basal medium was supplemented with 500 nM dexamethasone, 0.5 mM isobutylmethylxanthine (#I7018; Sigma-Aldrich), 50 mM indomethacin (#I7378; Sigma-Aldrich), and 10 mg/mL insulin (#I3536; Sigma-Aldrich). After another 2 days, the medium was replaced with a basal medium containing only insulin. The medium was changed every 2 days. The cells were cultured for 21 days for oil red O (#O0625; Sigma-Aldrich) staining. The presence of oil droplets was confirmed by staining the cells with 0.3% fresh oil red O solution for 30 min after fixation with 70% ethanol for 10 min.

RNA purification and quantitative real-time PCR (qRT-PCR)

Total RNA was prepared by using TRIzol reagent (Invitrogen, USA) in accordance with the manufacturer's instructions. A first-strand cDNA was synthesized from 1 µg of the total RNA by incubating for 1 h at 42 °C with Superscript III reverse transcriptase (Invitrogen, USA) following oligo (dT) priming. After the reverse transcription reaction, qRT-PCR was performed with a LightCycler480 system (Roche, Mannheim, Germany) using SYBR1Premix Ex Taq™ (Takara, Dalian, China) in accordance with the manufacturer's instructions. The conditions of RT-PCR were as follows:

denaturation at 95 °C for 10 s, 40 cycles at 95 °C for 10 s, and 60 °C for 30 s. The dissociation stage was added to the end of the amplification procedure. No non-specific amplification was determined by the dissociation curve. All of the amplifications were normalized by GAPDH. Data were analyzed by using comparison Ct ($2^{-\Delta\Delta Ct}$) method and expressed as fold change compared with respective control. Each sample was presented in mean with the standard error of triplicate. Primers were made by Sangon Biotech (Sangon Biotech, China). The primer sequences used in this study were as follows: miR-23b: forward, 5′-CTCAGGTGCTCT GGCTGCTTGGGT-3′; reverse, 5′-GCCAAGGTCGTG GTTGCGTGGT-3′; U6: forward, 5′-CTCGCTTCGGCA GCACA-3′; reverse, 5′-AACGCTTCACGAATTTGCGT-3′; GAPDH: forward, 5′-CCTCTGACTTCAACAGCGAC-3′; reverse, 5′-TCCTCTTGTGCTCTTGCTGG-3′; runx2: forward, 5′-GCCTTCAAGGTGGTAGCCC-3′; reverse, 5′CGT TACCCGC CATGACAGTA-3′; OCN: forward, 5′-GAA GCCCAGCGGTGCA-3′; reverse, 5′-CA CTACCTCGC TGCCCTCC-3′; ALP: forward, 5′-GAGTCGGACGTGTAC CGGA-3′; reverse, 5′-TGCCACTCCCACATTTGTCAC-3′.

Western blot

Cells were lysed on ice for 30 min in the lysis buffer containing 50 mM Tris-HCl, pH 7.4, 150 mM NaCl, 1% Nonidet P-40, and 0.1% SDS supplemented with protease inhibitors (10 mg/mL leupeptin, 10 mg/mL pepstatin A, and 10 mg/mL aprotinin). For Western blot analysis, 30 µg of protein sample was resolved on 10% SDS-PAGE and electrotransferred onto nitrocellulose membranes (Whatman, Piscataway, NJ). The primary antibodies used were anti-runx2 rabbit mAb (1:1000; Cell Signaling Technology, Inc.; no. 8486), GAPDH Rabbit mAb (1:1000; Cell Signaling Technology, USA; no. 5174). HRP-conjugated secondary antibodies were used at a 1:1000 dilution. The antigen-antibody complexes were made visible by using an enhanced chemiluminescence detection system (Millipore, Billerica, MA, USA) in accordance with the manufacturer's recommendations.

Alkaline phosphatase staining

Alkaline phosphatase (ALP) presence in the cell layers was assessed as follows. The cultured cells were rinsed with PBS three times and fixed with 4% paraformaldehyde for 10 min at 48 °C. The fixed cells were soaked in 0.1% naphthol AS-MX phosphate (Sigma-Aldrich, St. Louis, MO, USA) and 0.1% fast red violet LB salt (Sigma-Aldrich) in 56 mM 2-amino-2-methyl, 3-propanediol (pH 9.9; Sigma) for 10 min at room temperature, washed with PBS, and observed under a digital microscope.

Alizarin red staining

Cells were fixed in 70% ice-cold ethanol for 1 h and rinsed with ddH_2O. Cells were stained with 40 mM Alizarin red S (Sigma-Aldrich), pH 4.0, for 15 min while being gently agitated. Cells were rinsed five times with ddH_2O and then rinsed for 15 min with $1 \times$ PBS while being gently agitated.

Runx2 3′UTR cloning and luciferase assay

Runx2 mRNA 3′UTR containing the miR-23b-binding sequences for the human runx2 gene (gene ID 860) were amplified by PCR from human genomic DNA. The primer sequences used in this study were as follows: runx2-3′UTR-F: 5′-CCGCTCGAGAATTCCTCAGCAGTG GC-3′; runx2-3′UTR-R: 5′-GAATGCGGCCGCTAACAA AACCAAAAAAGCCATTTTATTG-3′. The PCR product was then subcloned into the XhoI-NotI site downstream of the stop codon in the pmiR-RB-REPORT empty vector (Guangzhou Ribo Bio Co., Ltd.). Binding-region mutations were achieved using a Quik-Change Site-Directed Mutagenesis Kit (Stratagene) following the manufacturer's instructions. Transient transfection of hBMSCs was carried out in six-well plates with Lipofectamine 2000 (Invitrogen) according to the manufacturer's instruction. The cells were co-transfected with 200 ng of the luciferase constructs and 50 ng of the pRL-TK (Promega, WI, USA) Renilla luciferase plasmid, and luciferase assays were performed with the dual-luciferase reporter assay system (Promega) according to the manufacturer's instructions. Luminescent signals were quantified by a luminometer (Glomax; Promega), and each value from the Renilla luciferase construct was normalized by firefly luciferase.

Construction of Ad-runx2 and Ad-EV

Adenoviruses encoding human runx2 (Ad-runx2) and empty plasmid (Ad-EV) were purchased from GenePharma (Shanghai; 1×10^9 TU/mL). hBMSCs were treated with Ad-EV and Ad-runx2 in combination with polybrene at the indicated MOI for 12 h, washed, and then maintained for 48–72 h prior to further analysis according to the manufacturer's instructions. Stable transfectants were selected by puromycin (Sigma-Aldrich) 72 h after lentivirus infection. For Ad-runx2 construction, the PCR products of runx2 were cloned into the EcoRI/BamHI site of ADV4 (CMV/IRES-GFP) using the following primers: 5′-TTGAAT TCGCAGAATTCTGTGAAAGTCGACAATT-3′ (sense); 5′-CGGGATCCTCCTCCCTTCAAAGCACTACCAC-3′ (antisense).

Histology and immunostaining

Bone tissue was fixed in 4% paraformaldehyde and embedded in paraffin. Paraffin blocks were sectioned at a thickness of 5 μm. Sections were deparaffinized in xylene and hydrated with graded ethanol. For immunohistochemistry, antigen retrieval was performed by incubating at 37 °C with 0.05% trypsin (pH 7.8). After blocking with 1% BSA, sections were incubated at 4 °C overnight with primary antibodies against runx2 (1:500; ab76956; Abcam, Cambridge, UK).

Animals

Male C57BL/6J mice 8 weeks old were purchased from Shanghai SLAC Laboratory Animal Co., Ltd., and housed at five per cage under standard conditions (12 h light/12 h dark cycle, 211°C controlled temperature). For miR-23b agomir injection, 8 mice were injected via caudal vein once a week (200 nmol/kg body weight) or with saline as a control for a period of 4 weeks and then were euthanized.

Bone histomorphometric analyses

We measured the structure of distal femurs with a SCANCO Medical mCT 40 scanner to produce the images and analyzed them with SCANCO evaluation software for segmentation, three-dimensional (3D) morphometric analysis, density, and distance parameters (SCANCO MedicalAG, Switzerland). 3D structural parameters analyzed included the following: total tissue volume (TV; contains both trabecular and cortical bone); trabecular bone volume per tissue volume (BV/TV); trabecular bone surface per tissue volume (BS/TV); bone mineral density (BMD); trabecular number (Tb.N); trabecular thickness (Tb.Th); trabecular separation (Tb.Sp). The bone histomorphometric parameters were calculated and expressed according to the standardized nomenclature for bone histomorphometry.

Statistical analysis

Statistically significant differences were determined using two-tailed Student's t test or ANOVA. Statistical significance was considered at $p < 0.05$. Data are presented as the mean $\pm$ SD.

Results

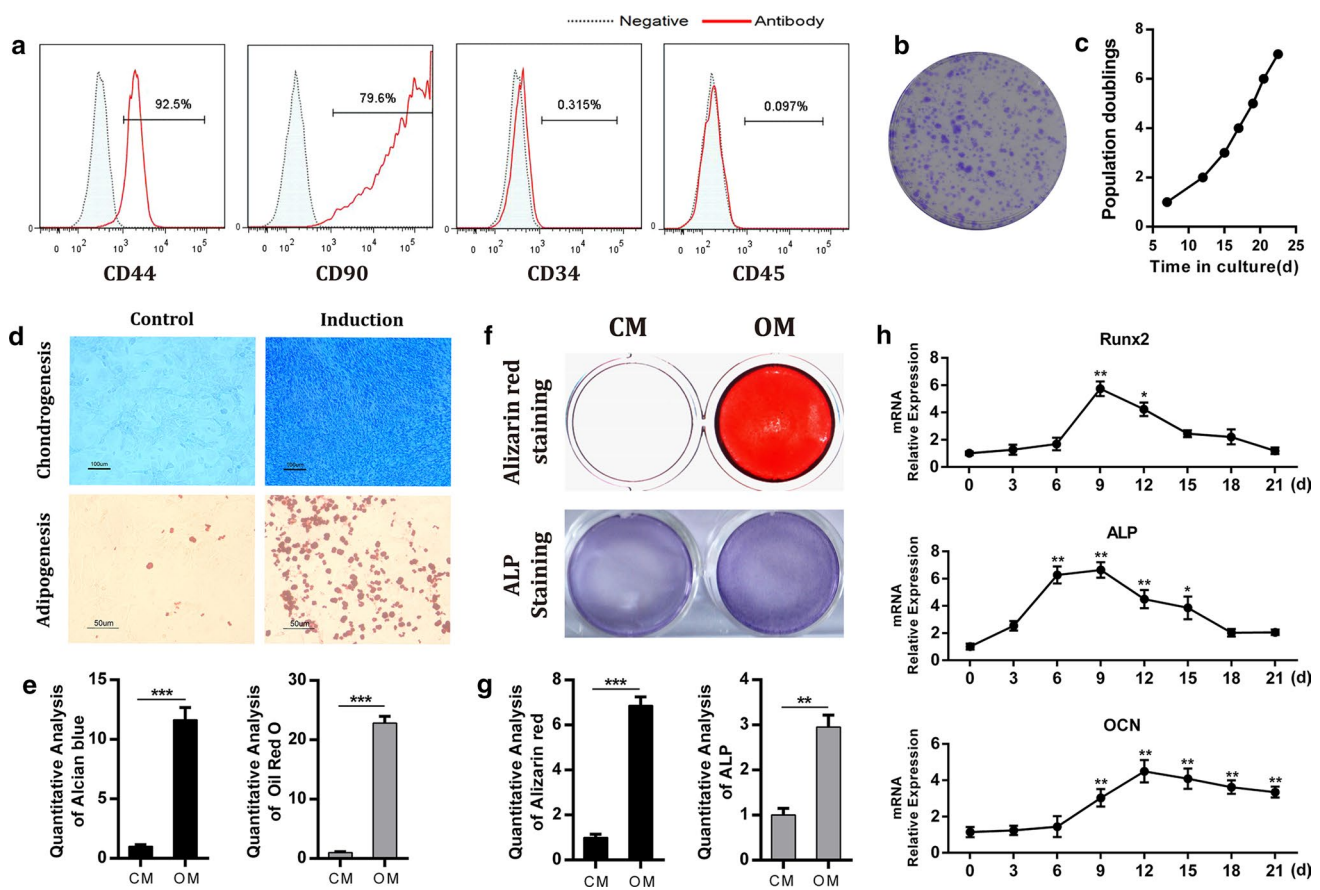## Identification and characterization of hBMSCs

The isolated hBMSCs positively expressed the MSC markers CD44 and CD90, but negatively expressed the hematopoietic marker CD34 and the leukocyte marker CD45

(Fig. 1a). Crystal violet staining indicated the colony-forming efficiency of hBMSCs (Fig. 1b). The cell growth curve further confirmed the results (Fig. 1c). The chondrogenic differentiation of hBMSCs was verified via alcian blue staining after 21 days of micromass culture. The micromass in the CM exhibited higher alcian blue staining compared with the control groups (upper part). The adipogenic differentiation capacity of hBMSCs was verified via oil red O staining. Lipid droplets were formed after 21 days of adipogenic induction. These droplets were fewer as observed in the control groups (Fig. 1d, e). Osteogenic differentiation assays indicated that most cells formed mineralized calcium deposits as confirmed by ALP staining and alizarin red S staining after culturing for 14 days in OM. By contrast, few mineralized calcium deposits were observed in the control groups

(Fig. 1f, g). qRT-PCR analysis showed increased expression of osteogenic specific genes, runx2, ALP, and OCN, at 3, 6, and 9 days after induction (Fig. 1h). These data validate that the isolated hBMSCs in our experiments possess the ability of rapid proliferation and multi-directional differentiation.

TNF-α inhibits hBMSC osteogenic differentiation and induces miR-23b expression

Osteogenic differentiation assays were assessed via ALP staining and alizarin red S staining after culturing for 14 days in OM with and without TNF-α (20 and 40 ng/ mL). The results showed that decreased ALP activity and fewer calcium deposits were obtained after osteogenic induction at a concentration of 40 ng/mL TNF-α compared


Fig. 1 Identification and characterization of human bone marrow-derived mesenchymal stem cells (hBMSCs). **a** Expression of hBMSC markers (CD44, CD90), hematopoietic stem cell marker (CD34) and leukocyte marker (CD45) on hBMSCs was measured by flow cytometry. hBMSCs highly expressed CD44 and CD90, but scarcely expressed CD34 and CD45. **b** The colony-forming efficiency of hBMSCs was confirmed by crystal violet staining. **c** The cell growth curve of hBMSCs. **d** The chondrogenesis and adipogenesis capabilities of hBMSCs were, respectively evaluated by alcian blue staining and oil red O staining after culturing for 21 days in chondrogenic medium or adipogenic medium. Scale bars, 100 μm (upper), 50 μm

(bottom). **e** The quantitative results of alcian blue staining and oil red O staining. **f** The osteogenesis capabilities of hBMSCs were evaluated by ALP staining and alizarin red staining after culturing for 14 days in osteogenic medium. **g** The quantitative results of ALP staining and alizarin red staining. **h** qRT-PCR analysis of the time course changes of runx2, alkaline phosphatase (ALP) and osteocalcin (OCN) mRNA levels (normalized by GAPDH) in hBMSCs during osteogenic medium-induced osteogenesis. Data represent the mean ± SEM of at least $n = 4$ independent experiments. *$p < 0.05$, **$p < 0.01$, ***$p < 0.001$. ns not significant, *CM* control medium, *OM* osteogenic medium

with the OM and 20 ng/mL groups (Fig. 2a, b). More calcium deposits were obtained in the OM + TNF-α + BAY 11-7082 group than in the OM + TNF-α + DMSO group after culturing for 14 days in OM via alizarin red S staining (Fig. 2c, d), suggesting that inhibition of NF-κB signaling abolished the inhibitory effect of TNF-α on BMSC osteogenic differentiation. The mRNA level of runx2 was analyzed via qRT-PCR under the conditions of CM or OM (OM + TNF-α, OM + TNF-α + BAY 11-7082). The results showed that decreased runx2 was detected in the OM + TNF-α group compared with the OM group, which was dramatically rescued after BAY 11-7082 treatment (Fig. 2e).

We hypothesized that runx2 might be regulated by miR-NAs through binding to its 3′UTR, resulting in decreased runx2 protein level and reduced osteoblast differentiation. Thus, we performed bioinformatic analyses using three miRNA target prediction software programs (i.e., TargetScan, miRDB, and miRanda) to screen for runx2-targeting miRNAs, and 8 miRNAs including miR-143, miR-103a, miR-221, miR-384, miR-23b, miR-154, miR-375, and miR-22 were finally acquired to potentially target the human runx2 3′UTR through multiple binding sites (Fig. 2f). The expression levels of aforementioned 8 miRNAs in hBMSCs stimulated with TNF-α for 24 h were analyzed via qRT-PCR. We then selected miR-23b to conduct the following
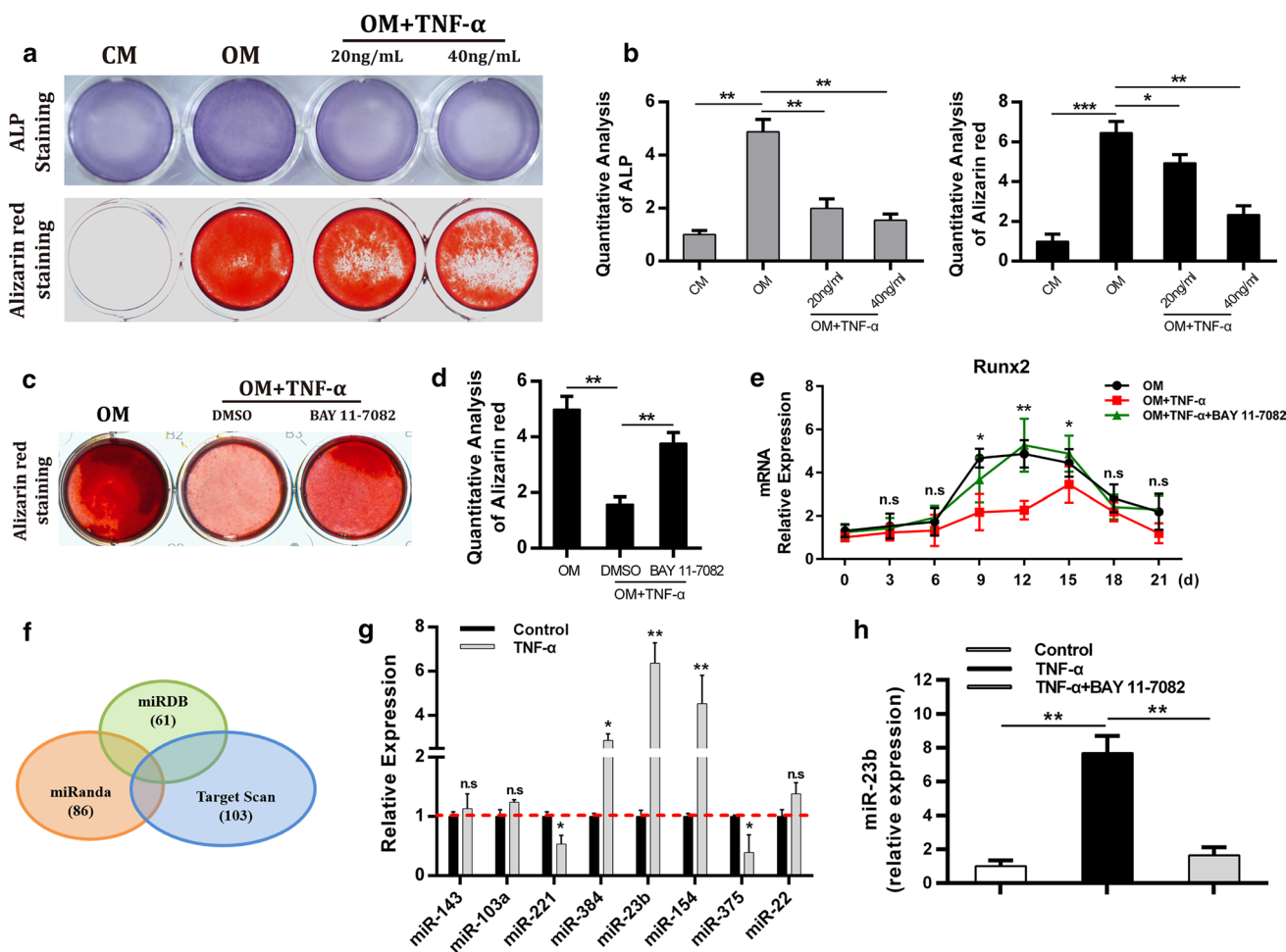
Fig. 2 TNF-α inhibits osteogenic differentiation and upregulates miR-23b expression. **a** Representative images of ALP staining and alizarin red staining of hBMSCs after culturing for 14 days in osteogenic medium with or without TNF-α (20 and 40 ng/mL). **b** The quantitative results of ALP staining and alizarin red staining. **c** Representative images of alizarin red staining of hBMSCs after culturing for 14 days in osteogenic medium contains TNF-α (40 ng/mL) with or without BAY 11-7082 (10 μM). **d** The quantitative result of alizarin red staining. **e** qRT-PCR analysis of the runx2 mRNA levels (normalized by GAPDH) in hBMSCs cultured with CM or OM (OM + TNF-α,

OM + TNF-α + BAY 11-7082), respectively. **f** Bioinformatic analysis using three miRNA target prediction software programs (TargetScan, miRDB and miRanda) to screen for runx2-targeting miRNAs. **g** The expression levels of eight predicted miRNAs in hBMSCs stimulated with TNF-α for 24 h. **h** qRT-PCR analysis of miR-23b expression in hBMSCs treated with TNF-α alone or combined with BAY 11-7082. Data represent the mean ± SEM of at least $n = 4$ independent experiments. $*p < 0.05$, $**p < 0.01$, $***p < 0.001$. *ns* not significant, *CM* control medium, *OM* osteogenic medium

experiments for its higher expression level induced by TNF-α (Fig. 2g). MiR-23b expression level in hBMSCs treated with TNF-α alone or combined with BAY 11-7082 was also analyzed via qRT-PCR. The result showed that miR-23b was dramatically induced by TNF-α, which was completely blocked by BAY 11-7082 (Fig. 2h). Taken together, our results demonstrate that TNF-α suppresses osteogenic differentiation of hBMSCs and upregulates miR-23b expression in hBMSCs.

Overexpression of miR-23b imitates the inhibitory effect of TNF-α on osteogenesis

Given that TNF-α inhibited hBMSC osteogenic differentiation, accompanied by a prompt upregulation of miR-23b, we then investigated the potential role of miR-23b during hBMSC osteogenic differentiation. Osteogenic differentiation assays were performed in miR-23b-overexpressing hBMSCs. Similar to the treatment with TNF-α, decreased ALP activity and fewer calcium deposits were obtained after osteogenic induction in the miR-23b-overexpressing hBMSCs compared with the negative controls (Fig. 3a, b). The in vivo role of miR-23b in osteogenesis was examined via caudal vein injection of agomir-23b into mice. In line with our in vitro results, injection of agomir-23b led to robust bone loss with marked decreases in volumetric bone mineral density and lower trabecular number accompanied by enlarged marrow cavity (Fig. 3c). Taking into account that bone is continuously being formed and resorbed to maintain mineral homeostasis and the structural integrity of the skeleton, we also assessed the osteoclast activity in mice injected with agomir-23b. The result showed that miR-23b had no effect on osteoclast activity in vivo (Fig. 3d). Moreover, osteoclastogenesis of bone marrow monocytes (BMMs) treated with miR-23b agomir or PBS was evaluated by TRAP staining, and the result showed that the number of TRAP+ cells was similar between the two groups (Fig. 3e), suggesting that miR-23b-induced bone loss was mainly attributed to impaired osteogenesis but not osteoclastogenesis. Collectively, miR-23b plays a negative regulatory role in hBMSC osteogenic differentiation, and enforced overexpression of miR-23b perfectly mimics TNF-α-reduced osteogenesis mainly by influencing the bone formation instead of bone resorption.

MiR-23b directly targets runx2 through a seed site in the 3′UTR

Next, we performed in vitro experiments to validate the direct binding of miR-23b to the runx2 3′UTR region. MiR-23b level was detected via qRT-PCR in hBMSCs transfected with agomir-23b or the negative control (NC), and found that miR-23b expression level was indeed elevated in the agomir-23b group (Fig. 4a), along with decreased runx2 expression level compared with the agomir-NC group (Fig. 4b). A similar result was obtained from western blot analysis of runx2 protein level in the agomir-23b group compared with the NC (Fig. 4c, d). In addition, the binding site of miR-23b in runx2 3′UTR is a highly conserved cross-species according to TargetScan analysis (Fig. 4e). To obtain further direct evidence that runx2 is a direct target of miR-23b, luciferase reporter constructs were generated by cloning either the wild type (WT) or a mutated (MT) portion of runx2 3′UTR (Fig. 4f) and then co-transfecting with agomir-23b or agomir-NC into hBMSCs. The ectopic expression of miR-23b markedly reduced the luciferase activity of the reporter with WT 3′UTR but not that of the MT reporter (Fig. 4g). Together, these results suggest that runx2 is a direct target of miR-23b in hBMSCs.

Ectopic expression of runx2 rescues miR-23b-mediated inhibition of osteogenic differentiation

To further confirm the essential role of runx2 in miR-23b-mediated inhibition of osteogenic differentiation, adenoviruses containing the entire coding sequence (CDS) of runx2 (Ad-*runx2*) were generated. The mRNA level of runx2 in hBMSCs infected with Ad-*runx2* or adenovirus containing Ad-EV was analyzed via qRT-PCR. Indeed, expression of runx2 was considerably elevated by Ad-*runx2* at the transcriptional and post-transcriptional level (Fig. 5a–c). Notably, miR-23b-mediated inhibition of osteogenic differentiation was powerfully rescued by ectopic expression of runx2 resulting from the infection of Ad-*runx2* (Fig. 5d, e). Meanwhile, the expression of runx2 was examined by western blot and the results showed that the amount of runx2 protein was dramatically raised in the panel adding Ad-*runx2* (Fig. 5f, g). These findings solidly demonstrated that miR-23b inhibited hBMSC osteogenic differentiation mechanically through suppression of runx2.

Activation of miR-23b leads to severe bone loss likely through its direct suppression of runx2

The in vivo role of miR-23b in bone homeostasis was examined via global delivery of agomir-23b alone or combined with Ad-*runx2* into mice (Fig. 6a). Similar to the results obtained from in vitro analysis, 4 weeks after injection, the bone mass of tibias in C57BL/6J mice from agomir-23b treatment group largely decreased compared with the saline-treated group, characterized by significant decline of several 3D microstructural parameters (BV/TV, BS/TV, BMD, Tb.N, and Tb.sp), but not Tb.Th (Fig. 6b, c). Encouragingly, ectopic expression of runx2 by injecting Ad-*runx2* absolutely eliminated the inhibitory effect of
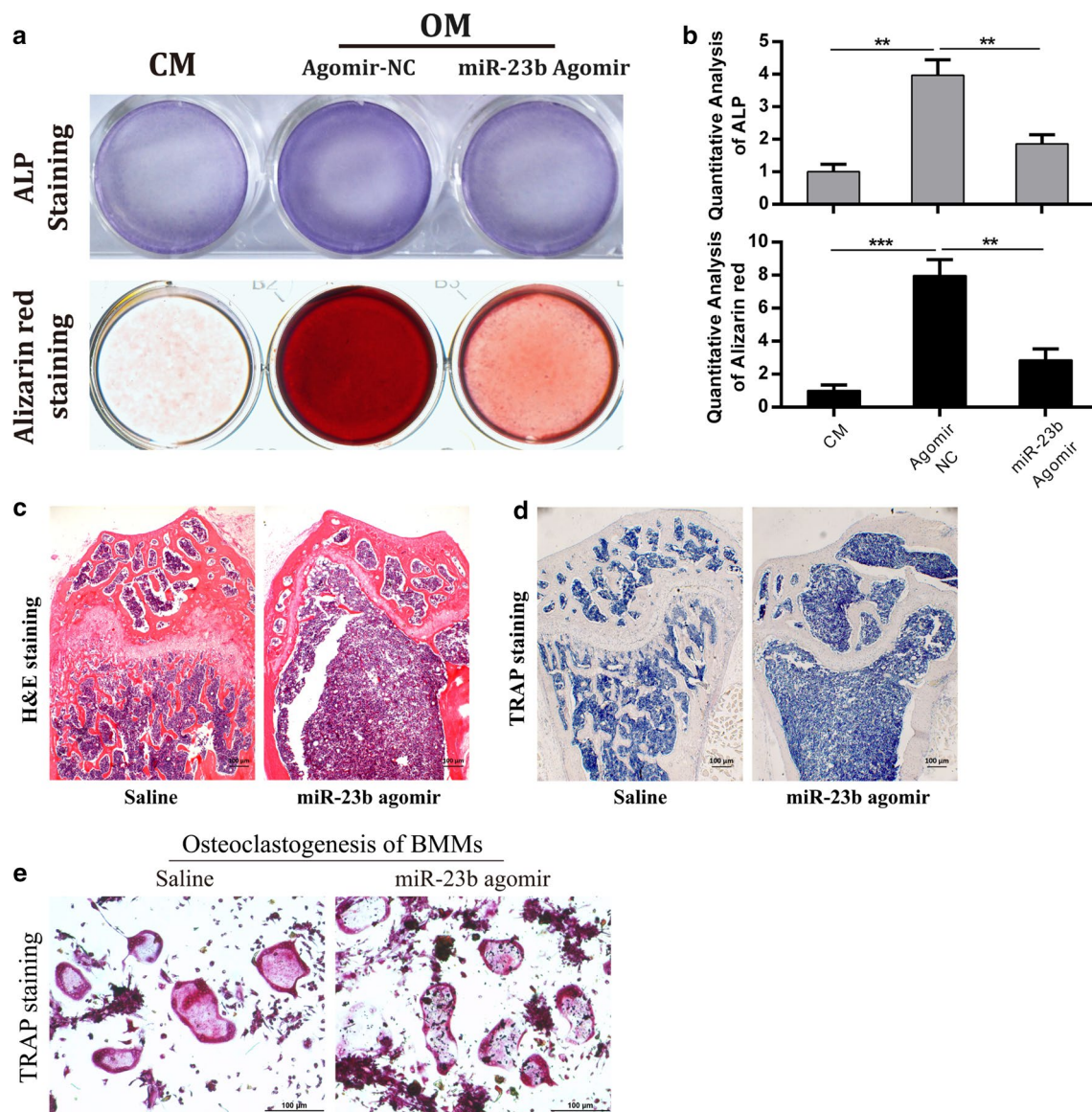
Fig. 3 Enforced overexpression of miR-23b impairs hBMSC osteogenesis in vitro and induces bone loss in vivo. **a** Representative images of alizarin red staining of hBMSCs after culturing for 14 days in osteogenic medium with agomir-NC or miR-23b agomir (100 nM). **b** The quantitative results of ALP staining and alizarin red staining. **c** H&E staining of tibia sections from mice injected with agomir-23b or saline via caudal vein. $n = 5$ per group. Scale bars, 100 μm. **d** TRAP staining of femur region from agomir-23b- or saline-treated mice. $n = 5$ per group. Scale bar, 100 μm. **e** Representative TRAP staining images of BMMs treated with agomir-23b or PBS. Scale bar, 100 μm. Data represent the mean ± SEM of at least $n = 4$ independent experiments. *$p < 0.05$, **$p < 0.01$, ***$p < 0.001$. *BMMs* bone marrow monocytes, *ns* not significant, *H&E* hematoxylin-eosin

miR-23b on bone mass (Fig. 6b, c). Indeed, Ad-runx2-GFP injection successfully elevated the expression of runx2 in bone (Fig. 6d, e). In summary, these observations reveal that activation of miR-23b causes severe bone loss in vivo and direct suppression of runx2 is responsible for its inhibitory regulation of bone formation.

Discussion

Osteoporosis, as an emerging worldwide epidemic, affects a large number of people worldwide, particularly older adults and post-menopausal women. Osteoporosis
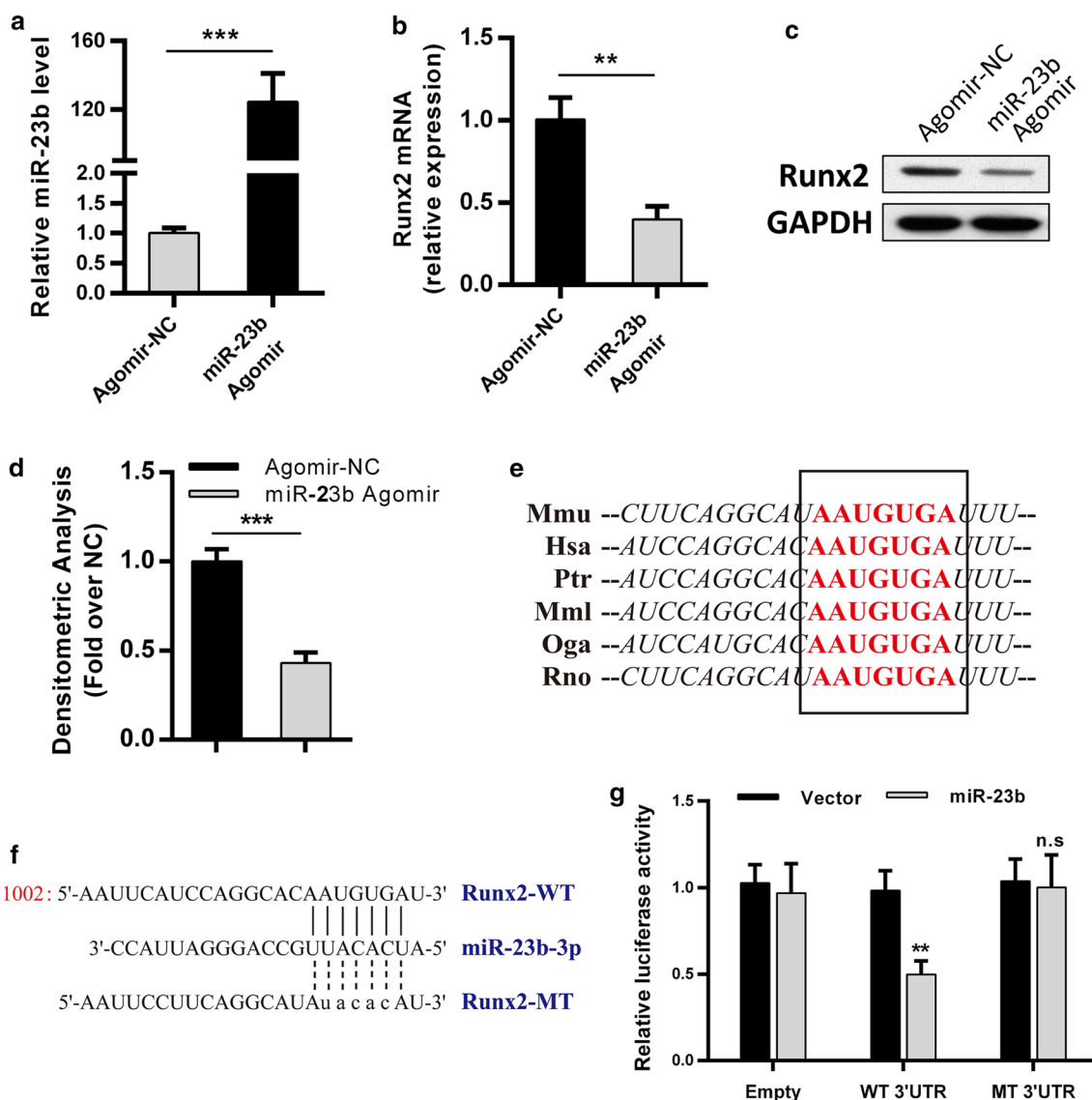
Fig. 4 MiR-23b directly targets runx2 in hBMSCs. **a** qRT-PCR analysis of miR-23b level in hBMSCs transfected with miR-23b agomir or negative control (agomir-NC). **b** The effect of agomir-NC or miR-23b agomir on the mRNA level of runx2 in hBMSCs. **c** The effect of agomir-NC or miR-23b agomir on the amount of runx2 protein in hBMSCs. **d** The quantitative result of western blot. **e** Cross-species conservation of the miR-23b seed sequence in the 3′UTR of runx2 mRNA. **f** Schematic representation of the runx2 3′UTR indicating the binding site of miR-23b. *WT* wild type, *MT* mutated. **g** hBMSCs were transfected with either pGL3 luciferase vector containing a fragment of runx2 3′UTR harbouring binding site for miR-23b, or the corresponding mutant constructs. Ectopic expression of miR-23b led to a remarkable reduction of the reporter luciferase activity with the wild-type 3′UTR but not that of the mutant reporter. Data represent the mean ± SEM of at least $n = 4$ independent experiments. *$p < 0.05$, **$p < 0.01$, ***$p < 0.001$. *ns* not significant

is characterized by decreased bone density and subdued strength, which eventually result in fragility fractures. On the basis of numerous associated investigations, TNF-α is a negative regulator of osteogenic differentiation and has been considered one of the major cytokines responsible for bone loss in many bone-related inflammatory diseases, such as rheumatoid arthritis and periodontitis [9, 10]. In this study, our results showed that decreased ALP activity and fewer calcium deposits were achieved after osteogenic induction with a concentration of 40 ng/mL

TNF-α. By contrast, the level of ALP activity and calcium deposits were rescued after BAY 11-7082 treatment, suggesting that the inhibitory effect of TNF-α on osteogenesis is NF-κB-dependent. Moreover, TNF-α largely induced miR-23b expression. In turn, overexpression of miR-23b inhibited ALP expression and the formation of calcium deposits in hBMSCs. On the other hand, miR-23b exhibited no effect on osteoclast activity. Our findings indicate that miR-23b is implicated in the negative regulation of TNF-α on BMSC osteogenic differentiation.
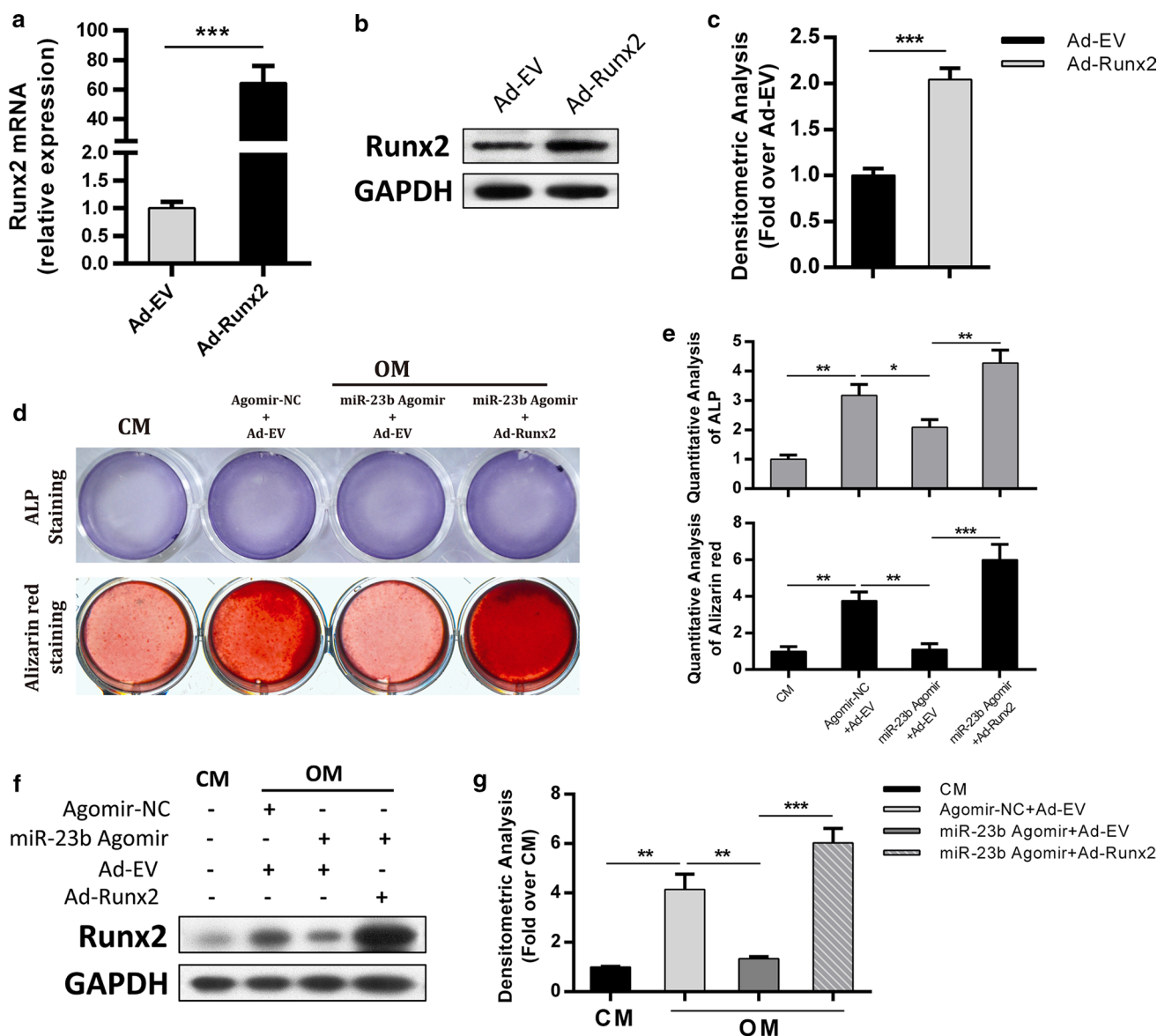
Fig. 5 Overexpression of runx2 counteracts the inhibition of miR-23b on hBMSC osteogenic differentiation in vitro. **a** qRT-PCR analysis of runx2 expression in hBMSCs infected with adenoviruses containing the entire CDS of runx2 (Ad-*runx2*) or empty vector (Ad-EV). **b** Western blot analysis of the runx2 protein amount in hBMSCs infected with Ad-*runx2* or Ad-EV. **c** The quantitative result of western blot. **d** Representative images of ALP staining and alizarin red staining of hBMSCs cultured in CM, and OM (agomir-NC + Ad-EV, miR-23b agomir + Ad-EV and miR-23b agomir + Ad-*runx2*), respectively. **e** The quantitative results of ALP staining and alizarin red staining. **f** Western blot analysis of the runx2 protein amount in hBMSCs treated as described above. Data represent the mean ± SEM of at least $n = 4$ independent experiments. *$p < 0.05$, **$p < 0.01$, ***$p < 0.001$. *ns* not significant

Runx2 is a critical transcriptional regulator of osteoblast differentiation and an important downstream target of BMP-2 [23–25]. It is specifically expressed in the cells of osteoblastic lineage at various differentiation stages ranging from immature mesenchymal osteochondro progenitors to mature osteoblasts. Runx2 expression is both necessary and sufficient for the differentiation of mesenchymal progenitor cells toward the osteoblastic lineage [23, 24]. In addition, runx2 enhances the transcription of all major

osteoblast-related genes, such as OCN, by specifically binding to the regulatory regions of the gene [26]. In the present study, we performed bioinformatic analyses using three miRNA target prediction software programs to screen for runx2-targeting miRNAs, and miR-23b was predicted to be a conserved miRNA binding with runx2 3′UTR. Further, we have fully validated the direct bond between miR-23b and runx2. The binding of miR-23b to runx2 3′UTR severely impaired the translation of runx2, eventually leading to
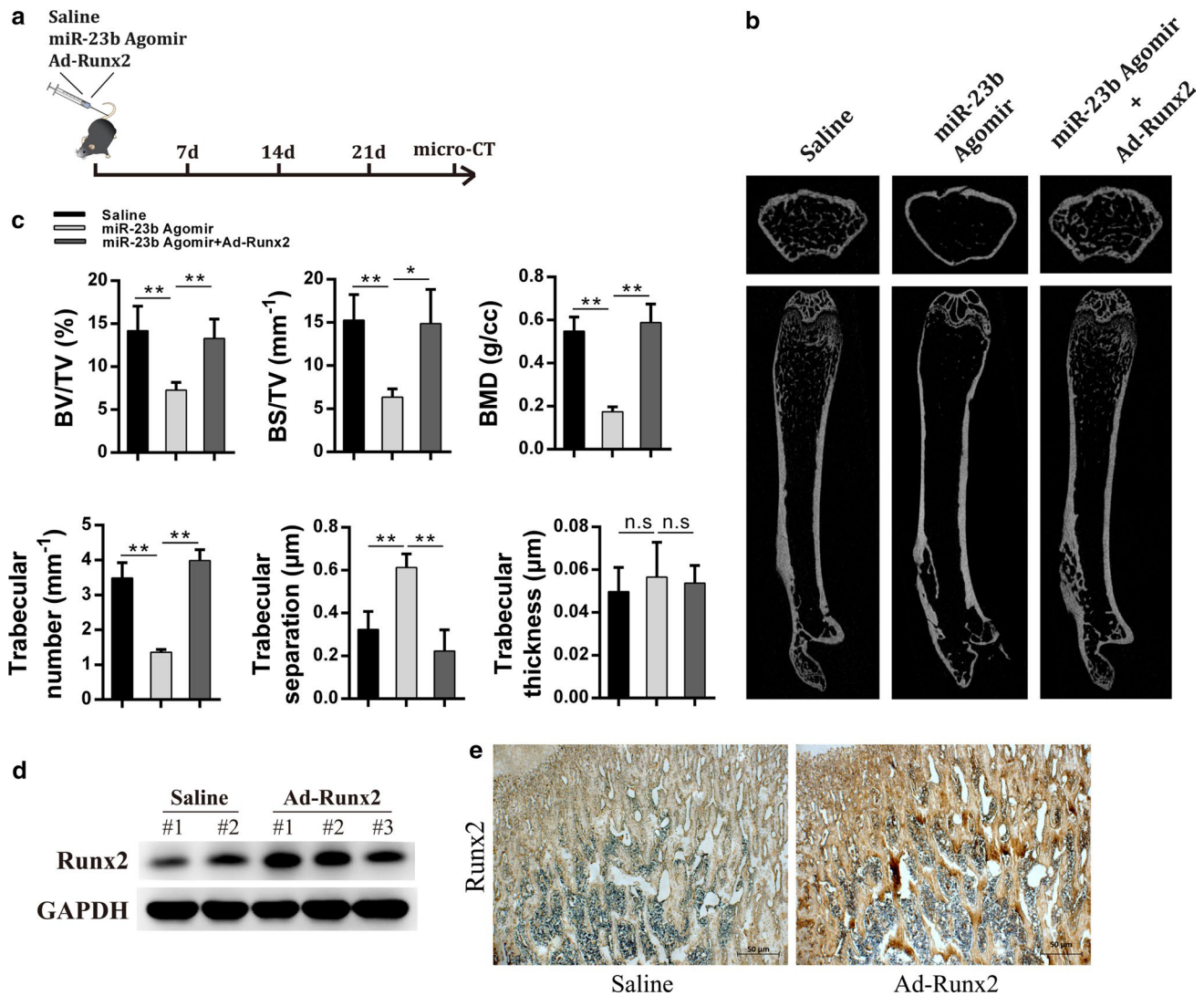
Fig. 6 Activation of miR-23b causes bone loss in vivo mainly through repressing runx2. **a** A schematic diagram illustrating the experimental design (for each group, $n = 6$ male C57BL/6J mice). **b** Representative micro-CT reconstructive images of femurs in C57BL/6J mice injected with PBS, miR-23b agomir, or miR-23b agomir + Ad-*runx2* through the tail vein. **c** Three-dimensional microstructural parameters of the tibias from C57BL/6J mice treated as described above. *BV/TV* trabecular bone volume per tissue volume, *BS/TV* trabecular bone surface per tissue volume, *BMD* bone mineral density, *Tb.N* trabecular number, *Tb.Th* trabecular thickness, *Tb. Sp* trabecular separation. **d** Western blot analysis of the runx2 protein amount in bone tissue obtained from mice injected with Ad-runx2-GFP or PBS. **e** Immunostaining of runx2 in bone tissue obtained from mice injected with Ad-runx2-GFP or PBS. Scale bar, 50 μm. Data represent the mean ± SEM of at least $n = 4$ independent experiments. *$p < 0.05$, **$p < 0.01$, ***$p < 0.001$. *ns* not significant

reduced osteogenesis. Thus, TNF-α-induced miR-23b upregulation, thereby suppressing runx2 expression, may be a new mechanism to explain the inhibition of TNF-α on osteogenic differentiation.

Recently, dozens of miRNA have emerged as important negative or positive regulators of post-transcriptional gene expression and are considered critical for osteogenesis [27–30]. In a recent study, miR-23b was found to be markedly downregulated in BMSCs of aged mice and humans, and regulated the balance between osteoblast and adipocyte differentiation in BMSCs mainly through the suppression of Tmem64, which was found to positively modulate osteoclast differentiation via the RANKL-mediated Ca^{2+} signaling pathway. Tmem64 primarily regulates the switch in the lineage commitment of MSCs to adipogenesis rather than to osteogenesis by suppressing β-catenin, the key Wnt signaling molecule. Thus, the negative regulatory role of miR-23b in MSC osteogenic differentiation described in this literature was mainly attributed to shifting MSCs to adipogenesis, but not influencing the osteogenic differentiation of MSCs directly. However, in this study, we identified miR-23b as a negative regulator of hBMSC osteogenic

differentiation directly through suppressing runx2. Our data also showed that activation of miR-23b in vivo causes severe bone loss. Therefore, miR-23b is crucial in regulating bone metabolism.

To our knowledge, this is the first study to report the regulatory role of miR-23b in osteogenic differentiation in inflammatory conditions in vitro and in vivo. Nevertheless, additional in-depth investigations should follow this preliminary study. For example, the signaling pathway involved in this process should be further clarified. Finally, our findings should be validated via patient treatment.

Author contributions LD and GH designed the study, performed the experiments, analysed the data and wrote the manuscript. LJ and CW performed the experiments and analysed the data. H-WN conceived the study, revised the manuscript and donated supplies and/or funding.

Compliance with ethical standards

Conflict of interest The authors declare no competing financial interests.

References

1. Gutschner T, Diederichs S (2012) The hallmarks of cancer: a long non-coding RNA point of view. RNA Biol 9:703–719
2. Rosenberg N, Rosenberg O, Soudry M (2012) Osteoblasts in bone physiology-mini review. Rambam Maimonides Med J 3:e0013
3. Li P, Yang YM, Sanchez S, Cui DC, Dang RJ, Wang XY, Lin QX, Wang Y, Wang C, Chen DF, Chen SY, Jiang XX, Wen N (2016) Deubiquitinase MYSM1 Is essential for normal bone formation and mesenchymal stem cell differentiation. Sci Rep 6:22211
4. Pittenger MF, Mackay AM, Beck SC, Jaiswal RK, Douglas R, Mosca JD, Moorman MA, Simonetti DW, Craig S, Marshak DR (1999) Multilineage potential of adult human mesenchymal stem cells. Science 284:143–147
5. Zhang W, Yang N, Shi XM (2008) Regulation of mesenchymal stem cell osteogenic differentiation by glucocorticoid-induced leucine zipper (GILZ). J Biol Chem 283:4723–4729
6. Duplomb L, Dagouassat M, Jourdon P, Heymann D (2007) Concise review: embryonic stem cells: a new tool to study osteoblast and osteoclast differentiation. Stem Cells 25:544–552
7. Nanes MS (2003) Tumor necrosis factor-alpha: molecular and cellular mechanisms in skeletal pathology. Gene 321:1–15
8. Gilbert L, He X, Farmer P, Boden S, Kozlowski M, Rubin J, Nanes MS (2000) Inhibition of osteoblast differentiation by tumor necrosis factor-alpha. Endocrinology 141:3956–3964
9. Beklen A, Ainola M, Hukkanen M, Gurgan C, Sorsa T, Konttinen YT (2007) MMPs, IL-1, and TNF are regulated by IL-17 in periodontitis. J Dent Res 86:347–351
10. Choy EH, Panayi GS (2001) Cytokine pathways and joint inflammation in rheumatoid arthritis. N Engl J Med 344:907–916
11. Ye X, Huang H, Zhao N, Zhang J, Yang P (2016) Inhibition of Runx2 signaling by TNF-alpha in ST2 murine bone marrow stromal cells undergoing osteogenic differentiation. In vitro Cell Dev Biol Anim 52:1026–1033
12. Malysheva K, de Rooij K, Lowik CW, Baeten DL, Rose-John S, Stoika R, Korchynskyi O (2016) Interleukin 6/Wnt interactions in rheumatoid arthritis: interleukin 6 inhibits Wnt signaling in synovial fibroblasts and osteoblasts. Croat Med J 57:89–98
13. Thomas M, Lieberman J, Lal A (2010) Desperately seeking microRNA targets. Nat Struct Mol Biol 17:1169–1174
14. Esteller M (2011) Non-coding RNAs in human disease. Nat Rev Genet 12:861–874
15. Itoh T, Takeda S, Akao Y (2010) MicroRNA-208 modulates BMP-2-stimulated mouse preosteoblast differentiation by directly targeting V-ets erythroblastosis virus E26 oncogene homolog 1. J Biol Chem 285:27745–27752
16. Schaap-Oziemlak AM, Raymakers RA, Bergevoet SM, Gilissen C, Jansen BJ, Adema GJ, Kögler G, le Sage C, Agami R, van der Reijden BA, Jansen JH (2010) MicroRNA hsa-miR-135b regulates mineralization in osteogenic differentiation of human unrestricted somatic stem cells. Stem Cells Dev 19:877–885
17. Huang J, Zhao L, Xing L, Chen D (2010) MicroRNA-204 regulates Runx2 protein expression and mesenchymal progenitor cell differentiation. Stem Cells 28:357–364
18. Jeong BC, Kang IH, Hwang YC, Kim SH, Koh JT (2014) MicroRNA-194 reciprocally stimulates osteogenesis and inhibits adipogenesis via regulating COUP-TFII expression. Cell Death Dis 5:e1532
19. Li H, Li T, Fan J, Li T, Fan L, Wang S, Weng X, Han Q, Zhao RC (2015) miR-216a rescues dexamethasone suppression of osteogenesis, promotes osteoblast differentiation and enhances bone formation, by regulating c-Cbl-mediated PI3K/AKT pathway. Cell Death Differ 22:1935–1945
20. Hu R, Li H, Liu W, Yang L, Tan YF, Luo XH (2010) Targeting miRNAs in osteoblast differentiation and bone formation. Expert Opin Ther Targets 14:1109–1120
21. Guo Q, Chen Y, Guo L, Jiang T, Lin Z (2016) miR-23a/b regulates the balance between osteoblast and adipocyte differentiation in bone marrow mesenchymal stem cells. Bone Res 4:16022
22. Chen C, Tang Z, Song Q, Yang M, Shi Q, Weng Y (2016) Down-regulated microRNA-23b promotes BMP9-mediated osteogenesis in C2C12 myoblast cells by targeting Runx2. Mol Med Rep 13:2492–2498
23. Dalle Carbonare L, Innamorati G, Valenti MT (2012) Transcription factor Runx2 and its application to bone tissue engineering. Stem Cell Rev 8:891–897
24. Komori T (2010) Regulation of bone development and extracellular matrix protein genes by RUNX2. Cell Tissue Res 339:189–195
25. Phimphilai M, Zhao Z, Boules H, Roca H, Franceschi RT (2006) BMP signaling is required for RUNX2-dependent induction of the osteoblast phenotype. J Bone Miner Res 21:637–646
26. Xiao G, Jiang D, Ge C, Zhao Z, Lai Y, Boules H, Phimphilai M, Yang X, Karsenty G, Franceschi RT (2005) Cooperative interactions between activating transcription factor 4 and Runx2/Cbfa1 stimulate osteoblast-specific osteocalcin gene expression. J Biol Chem 280:30689–30696
27. Lee WY, Li N, Lin S, Wang B, Lan HY, Li G (2016) miRNA-29b improves bone healing in mouse fracture model. Mol Cell Endocrinol 430:97–107
28. Peng S, Gao D, Gao C, Wei P, Niu M, Shuai C (2016) MicroRNAs regulate signaling pathways in osteogenic differentiation of mesenchymal stem cells (review). Mol Med Rep 14:623–629

29. Huang C, Geng J, Jiang S (2017) MicroRNAs in regulation of osteogenic differentiation of mesenchymal stem cells. Cell Tissue Res 368:229–238

30. Yoshizuka M, Nakasa T, Kawanishi Y, Hachisuka S, Furuta T, Miyaki S, Adachi N, Ochi M (2016) Inhibition of microRNA-222 expression accelerates bone healing with enhancement of osteogenesis, chondrogenesis, and angiogenesis in a rat refractory fracture model. J Orthop Sci 21:852–858